Cavitation-Induced Fracture Causes Nanocorrugations in Brittle Metallic Glasses

I. Singh,[1] R. Narasimhan,[1,*] and Upadrasta Ramamurty[2]
[1]Department of Mechanical Engineering, Indian Institute of Science, Bangalore 560012, India
[2]Department of Materials Engineering, Indian Institute of Science, Bangalore 560012, India
(Received 16 March 2016; revised manuscript received 20 May 2016; published 22 July 2016)

Brittle metallic glasses exhibit a unique and intriguing fracture morphology of periodic nanocorrugations whose spacing and amplitude are of the order of tens of nanometers. We show through continuum simulations that they fail by spontaneous and simultaneous cavitation within multiple weak zones arising due to intrinsic atomic density fluctuations ahead of a notch tip. Dynamic crack growth would then occur along curved but narrowly confined shear bands that link the growing cavities. This mechanism involves little dissipation and also explains the formation of nanocorrugations.

DOI: 10.1103/PhysRevLett.117.044302

Metallic glasses (MGs) can be classified based on their mechanical behavior as ductile or brittle. While the former exhibit profuse shear banding near a crack or notch tip and consequently have high fracture toughness, $K_{Ic} \sim$ 50–100 MPa $m^{1/2}$ [1–4], the latter show negligible crack tip plasticity, at least at the macroscopic scale, and possess a low $K_{Ic} \sim 1$–5 MPa $m^{1/2}$ [5–10]. High magnification imaging of the fracture surfaces of brittle MGs shows regular and parallel stripes, commonly referred to as nanocorrugations (NCs), perpendicular to the crack propagation direction [6–12]. Atomic force microscopy (AFM) reveals that NCs have wavelengths λ ranging from 30 to 120 nm and heights between 3 and 10 nm [7,9,11]. It is generally accepted that the physical origin of NCs lies in cavitation within an amorphous matrix [6–11]. Yet, the following questions related to the physics of NC formation remain unanswered. What drives spontaneous cavity nucleation ahead of a crack tip, given that the peak hydrostatic stress attained is considerably lower than the critical level for cavitation in elastoplastic solids [13–16]? Is there something specific about the mechanism of cavity coalescence in brittle MGs, which results in the observed NCs? Finally, how does the toughness of the MG relate to features like NC spacing? It must be mentioned that cavitation has also been reported in oxide glasses [17–23], although the issues posed above concerning the formation of NCs and their relationship to cavity coalescence are unique to MGs.

Molecular dynamics (MD) simulations [13,24] have established that brittle MGs exhibit large atomic density fluctuations and multiple cavity nucleation occurs in regions of reduced density (and strength). This has indeed been confirmed from recent continuum analyses that model brittle MGs as heterogeneous plastic solids with distributed weak zones (WZs) [25,26]. Numerical simulations using special plasticity theories combined with level-set or finite element (FE) methods have been undertaken by Rycroft and Bouchbinder [27] and Henann and Anand [28] to model cavity nucleation ahead of a crack tip in MGs. However, these studies do not explain NC formation; they predict void initiation irrespective of the initial structural state [27] and assume a low ratio of cavitation stress to the yield strength that is spatially uniform [28]. Importantly, they have not captured the unique cavitation behaviors of brittle MGs as seen in MD simulations such as the simultaneous and synergistic cavity nucleation in several WZs that is insensitive to a preexisting void [13,24]. In the present Letter, we attempt to gain key insights on the cavitation-induced fracture processes and NC formation in brittle MGs via 2D plane strain, FE simulations of small scale yielding (SSY) that are guided by prior experimental [7,10] and atomistic modeling [13]. Excluding free surface effects, hydrostatic stresses near the crack front are uniform and the plastic zone size in brittle MGs is small; thus, the 2D SSY model is justified.

We simulate the SSY problem by considering a circular domain of radius R_o, containing a semicircular notch (diameter $b_o = 3.3 \times 10^{-3}\ R_o$) and prescribe the mode-I, linear elastic stress intensity factor based K field [29] at its outer boundary [27,28]. We introduce three equispaced (center-to-center distance L_o) WZs (WZ-I, WZ-II, and WZ-III) ahead of the notch tip [see Fig. 1(a)] to represent the density fluctuations seen in brittle MGs [13,24]. This model is justified since the above fluctuations contain few distinct wavelengths [13]. In order to trigger cavitation inside the WZs, infinitesimally small circular voids (with radii $r_o = 0.013L_o$ as necessitated by computational limitations) are placed at their center. During loading, cavitation is marked by the sudden and rapid growth of these voids [15]. Also, guided by the observed height-to-spacing ratio of the NCs (about 1/10 to 1/7 [7–11]), the initial radius r_w of the weak zones is taken as $0.13L_o$. We model only the upper half plane due to mode-I symmetry and employ a special plasticity theory [30], which has been shown to accurately capture the mechanical and fracture response of MGs [3,31–33]. It is based on the Mohr-Coulomb criterion proposed for MGs [34] and represents

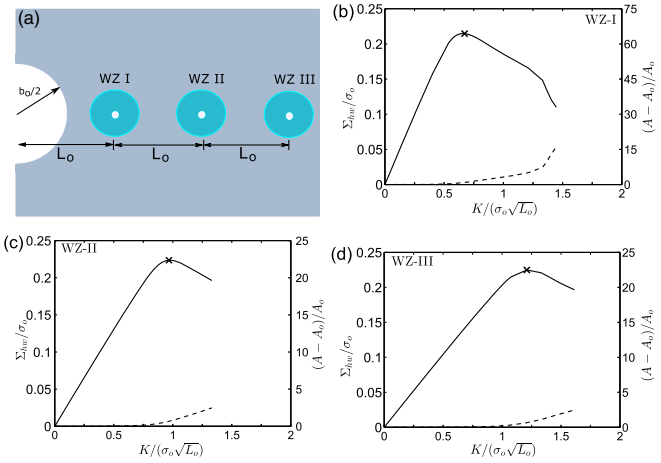

FIG. 1. (a) Schematic showing three weak zones indicated as WZ-I, WZ-II, and WZ-III ahead of a notch tip. Variation of the normalized macroscopic hydrostatic stress Σ_{hw}/σ_o and relative increase in the corresponding void areas $(A-A_o)/A_o$ with $K/(\sigma_o\sqrt{L_o})$ corresponding to the weak zone (b) WZ-I, (c) WZ-II, and (d) WZ-III for $\sigma_{ow}/\sigma_o = 0.1$. The stage at which cavitation occurs in the respective weak zones is marked by "cross" symbols.

free volume as an internal variable given by $\eta = \ln(\det \mathbf{F}^p)$, where $\mathbf{F}^p$ is the plastic deformation gradient. This evolves due to shear induced dilatation [35] and attains a saturation level η_{cv} while the cohesion c decays smoothly from an initial value c_o to reach a limiting value of c_{cv}. (Shear induced dilatation is countered by structural relaxation leading to saturation in η [35].) The values of η_{cv} and c_{cv} are taken as 0.005 and $0.9c_o$, while the friction coefficient μ, elastic modulus E, and Poisson's ratio ν are chosen as 0.15, $57.4c_o$, and 0.36, respectively, which are all representative of MGs [3,30]. We consider three ratios of tensile yield strength {which is given by $2c_o/[\cos\phi+\mu(1+\sin\phi)]$, where $\phi = \tan^{-1}(\mu)$} of the weak zones to that of the matrix ($\sigma_{ow}/\sigma_o = 0.1$, 0.3, and 0.6). More details of the constitutive model, material parameters, and FE modeling aspects may be found in Refs. [3,30–32] as well as in the Supplemental Material [36].

Figures 1(b)–1(d) show the variation of the normalized macroscopic hydrostatic stress Σ_{hw}/σ_o in the three WZs, along with the relative increase in corresponding void areas $(A-A_o)/A_o$ with the load parameter $K/(\sigma_o\sqrt{L_o})$ for $\sigma_{ow}/\sigma_o = 0.1$. Note that $(A-A_o)/A_o$ does not change in any significant manner until the peak in Σ_{hw}/σ_o is attained in the WZs and thereafter increases rapidly signifying cavitation [14,15,25,26]. Importantly, the peak in Σ_{hw}, which corresponds to the cavitation stress, is of the order of $0.2\sigma_o$ to $0.25\sigma_o$. This enhances to around $0.56\sigma_o$ and $1.1\sigma_o$ when σ_{ow}/σ_o is increased to 0.3 and 0.6, respectively. These values are markedly low vis-a-vis cavitation stress levels of homogeneous solids ($\sim 2.7\sigma_o$ for $\sigma_o/E = 0.03$ [14,15]). The low hydrostatic stress for multiple and simultaneous cavitation ahead of the crack tip before it begins to grow (see also Fig. 2) is consistent with MD simulations [13,24].

In Figs. 2(a)–2(f), we show contour plots of the maximum principal logarithmic plastic strain $\log\lambda_1^p$ for different values of $K/(\sigma_o\sqrt{L_o})$ corresponding to $\sigma_{ow}/\sigma_o = 0.1$ (see Ref. [36] for movies of the simulations). The bottom halves in these plots are mirror images of the upper halves. In

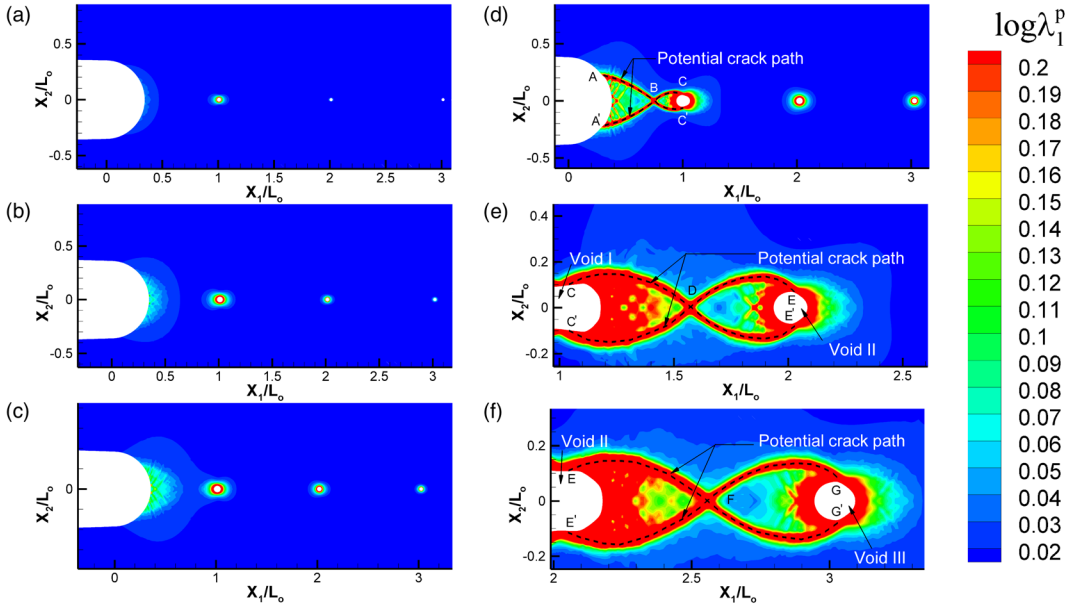

FIG. 2. Contour plots of the maximum principal logarithmic plastic strain $\log\lambda_1^p$ at $K/(\sigma_o\sqrt{L_o})$ of (a) 0.67, (b) 0.96, (c) 1.21, (d) 1.45, (e) 2.09, and (f) 2.37 for $\sigma_{ow}/\sigma_o = 0.1$. Potential crack paths along which crack propagation is likely to occur are indicated by black dashed lines. A simulation movie is available in the Supplemental Material [36].

Fig. 2(a), which pertains to the stage when cavitation occurs in WZ-I, plastic strain near the notch root is negligible. With increasing K, plastic strain accumulates around void I and it grows rapidly [see also Fig. 1(b)], while yielding commences near the notch tip as well [Fig. 2(b)]. Also, voids II and III start to expand following cavitation in WZ-II and WZ-III [Figs. 2(b) and 2(c), respectively]. It must be noted from Fig. 2(c) that even after cavitation has occurred in all three WZs, $\log \lambda_1^p < 0.1$ near the notch root. Thus, cavitation may occur inside many weak zones before considerable plastic strain develops near the notch tip when σ_{ow}/σ_o is low.

As loading progresses further, discrete bands of localized plastic deformation form near the notch surface, see Fig. 2(d). In striking contrast to ductile crystalline metals, where coalescence of void I with the notch would have occurred by internal ligament necking [38] accompanied by large plastic dissipation, a totally different mode of void coalescence involving two narrow curved shear bands (SBs) A-B-C and A'-B-C' is seen linking void I with the notch surface in Fig. 2(d). Failure would take place by crack propagation within these SBs, once the plastic strain [3,30] or free volume [39,40] exceeds a critical level. If the level of critical plastic strain is taken as 0.2 [3], then the above failure process would have linked void I with the notch in Fig. 2(d). Thus, the coalescence of voids in brittle MGs involves an abrupt termination of void growth through failure along curved SBs. This has important implications on the fracture morphology and formation of NCs on the fracture surface of brittle MGs.

Figures 2(e) and 2(f) show that the failure mechanism described above repeats, linking the voids further ahead of the notch tip (see also the simulation movie in Ref. [36]). Thus, curved SBs C-D-E and C'-D-E' (with $\log \lambda_1^p > 0.2$) can be seen bridging the ligament between voids I and II in Fig. 2(e), while similar bands labeled as E-F-G and E'-F-G' may be perceived in Fig. 2(f) linking voids II and III. It must be noted from Fig. 2 that the width of the fracture process zone (transverse to the crack propagation direction) wherein plastic deformation is confined is of the order of $2r_w$ (which is quite small, ~10 to 20 nm, as discussed below). It is important to recognize here that this confinement arises due to the interplay between the nucleation of cavities and their subsequent linking through curved SBs. By contrast, ductile MGs exhibit profuse shear banding extending to significant distances (of the order of few hundred microns) above and in front of a crack tip [1]. This is due to the lack of cavitation within the matrix in them [13]; instead, extensive plasticity predominates through shear banding. The apparent increase in K before the curved SBs C-D-E and E-F-G form to link voids I, II and voids II, III [Figs. 2(e) and 2(f)] is because the actual failure by dynamic crack propagation from the notch root has not been simulated in the present work.

Thus, the mechanism of crack growth in brittle MGs involves the following three sequential steps. First, cavities nucleate in WZs (of reduced atomic density) ahead of the crack tip when the macroscopic hydrostatic stress within them attains a critical level and start growing unstably [25,26]. Second, curved SBs form linking the current crack tip with the nearby cavity. Finally, as plastic strain and free volume accumulate rapidly within these SBs, dynamic failure takes place facilitating further extension of the crack. This mechanism is distinct vis-a-vis ductile crystalline metals wherein cavities nucleate by the debonding or cracking of inclusions, grow stably owing to strain hardening of the matrix, and coalesce generally through necking, which mandates substantial energy dissipation and hence imparts high toughness [38,41,42]. In contrast, the spontaneous nucleation and unstable growth of cavities followed by linking through confined SBs (triggered by free volume induced softening) does not consume much energy as there is no diffuse plasticity. That is why MGs that fail through this mechanism are brittle [6–10].

In order to clearly ascertain the failure path, we conducted some simulations by modeling the entire domain and spatially perturbing the cohesion through different random distributions. It was found that curved SB A-B-C' forms before A-B-C [Fig. 3(a)] implying that the level of K or energy release rate required for crack propagation to occur along the former is lower than along the latter. The above process is expected to repeat as more cavities link with the crack tip leading to the crack profile illustrated in Fig. 3(b), which is curved and periodic with wavelength L_o and a height h of $1-2\ r_w$ (i.e., $0.25\ L_o$). This is consistent with the results of fracture surface imaging through AFM [7–11]. However, it must be mentioned that the issue of preference between the above two potential SB-guided crack paths requires further investigation. It is linked to initial fluctuations as well as the level of energy release rate required to operate them. To gain further insight, we considered a representative volume element located within the zone of high hydrostatic stress ahead of the crack tip (see Ref. [36]) containing several distributions of WZs with different strengths and spacings. We subjected this representative volume element to a macroscopic stress ratio of 0.7, typical of the stress state ahead of a crack tip in an elastic-plastic solid [43,44]. We found that cavitation always occurs in the WZs with the lowest strength and the cavities link up through curved SB paths [36].

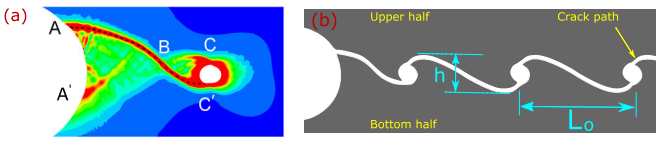

FIG. 3. (a) Contours of plastic strain obtained from a simulation of the full domain showing a curved SB linking the notch tip with void I. (b) Schematic depicting the potential crack path deduced on the basis of (a).

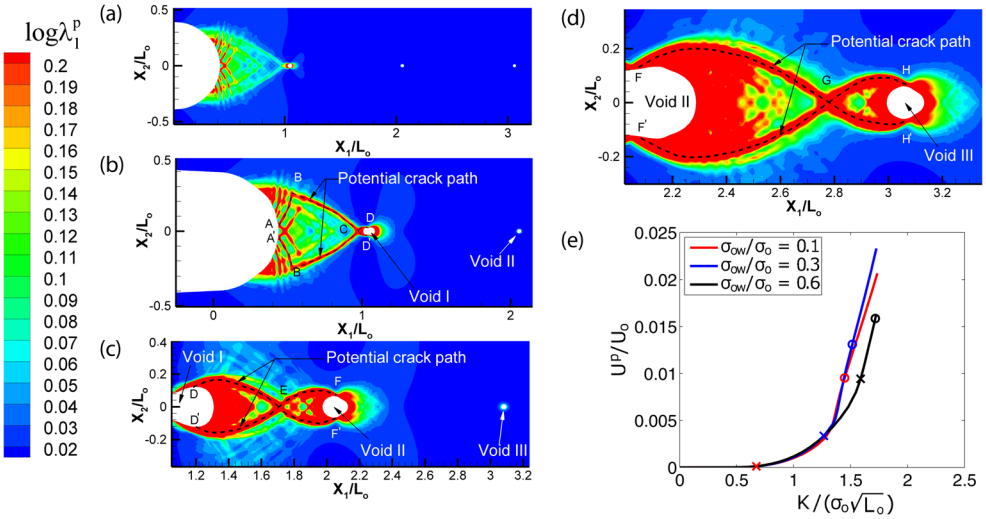

FIG. 4. Contour plots of the maximum principal logarithmic plastic strain $\log\lambda_1^p$ at $K/(\sigma_o\sqrt{L_o})$ of (a) 1.58, (b) 1.72, (c) 2.34, and (d) 2.52 for $\sigma_{ow}/\sigma_o = 0.6$. The potential crack paths along which crack propagation is likely to occur are indicated by black dashed lines. (e) Variation of the plastic work U^p per unit thickness normalized by $U_o = \sigma_o L_o^2$ with $K/(\sigma_o\sqrt{L_o})$ for different values of σ_{ow}/σ_o. The stage at which cavitation occurs in WZ-I is indicated by the "cross" symbol and that pertaining to fracture initiation (when the notch tip links with void I following failure in a curved SB) is indicated by the "circle" symbol.

Figures 4(a)–4(d) display contour plots of $\log\lambda_1^p$ corresponding to a higher $\sigma_{ow}/\sigma_o = 0.6$. Figure 4(a), which pertains to the stage when cavitation occurs in WZ-I, shows more perceptible shear banding near the notch root as compared to Fig. 2(a). However, the failure mode does not change with SBs sequentially linking the notch root with void I [bands *A*-*B*-*C*-*D* and *A*′-*B*′-*C*-*D*′ in Fig. 4(b)], void I with void II [bands *D*-*E*-*F* and *D*′-*E*-*F*′ in Fig. 4(c)], and void II with void III [bands *F*-*G*-*H* and *F*′-*G*-*H*′ in Fig. 4(d)].

The plastic work per unit thickness U^p, normalized by $U_o = \sigma_o L_o^2$, in the heterogeneous aggregate is plotted against $K/(\sigma_o\sqrt{L_o})$ in Fig. 4(e) for various values of σ_{ow}/σ_o. It reveals that U^p at cavitation in WZ-I (marked by "cross") is negligible for low $\sigma_{ow}/\sigma_o = 0.1$, but increases strongly with elevation in WZ strength owing to the enhanced plasticity near the notch surface. Also, U^p/U_o and K at crack initiation (when the notch tip links with void I following failure in a curved SB) increase or the fracture process becomes more dissipative with elevation in σ_{ow}/σ_o. To contrast this with a ductile MG, we performed a SSY simulation with no WZs and cavitation-induced failure. Multiple SBs develop and U^p/U_o when plastic strain exceeds 0.2 over a distance L_o from the notch is 0.21, which is much higher than that shown in Fig. 4(e).

Further, the present simulations indicate that K_{Ic} of brittle MGs would enhance with $\sigma_o\sqrt{\lambda}$ if λ is identified with L_o, as suggested by Fig. 3(b). This is corroborated by the experimental data presented by Wang *et al.* [9] for a variety of brittle MGs. For example, K_{Ic} increases from 1 to 5 MPa m$^{1/2}$ as $\sigma_o\sqrt{\lambda}$ is enhanced from ~0.1 ($Mg_{65}Cu_{20}Ni_5Gd_{10}$) to 0.7 MPa m$^{1/2}$ ($Fe_{73.5}Cu_1Nb_3Si_{13.5}B_9$). These observations indicate that the brittle cavitation-induced fracture mechanism can be suppressed by increasing λ and/or σ_{ow}/σ_o through tuning the chemical composition [24]. The data presented in Fig. 4 for K_c are however lower than the above values [9], owing to the specific assumptions about the constitutive parameters and the failure strain made in this work.

In summary, continuum simulations of crack initiation in brittle MGs have been performed. The results show that a three-step process leads to the catastrophic fracture observed in these materials: (i) simultaneous and unstable cavitation in WZs ahead of a crack tip when a critical level of hydrostatic stress is attained, (ii) linking of cavities with the crack tip or other cavities by curved and highly confined SBs, and (iii) rapid failure by dynamic crack propagation in the curved bands. This mechanism also helps explain the unique NC features observed in fractographs of these materials. It can be suppressed and, in turn, fracture toughness can be enhanced by increasing the wavelength and/or reducing the amplitude of the nanoscale strength fluctuations through changes in chemical composition.

R. N. and U. R. would like to thank the Department of Science and Technology (Government of India) for financial support under the JC Bose Fellowship scheme.

*narasi@mecheng.iisc.ernet.in

[1] K. M. Flores and R. H. Dauskardt, Scr. Mater. **41**, 937 (1999).

[2] J. Schroers and W. L. Johnson, Phys. Rev. Lett. **93**, 255506 (2004).

[3] P. Tandaiya, U. Ramamurty, and R. Narasimhan, J. Mech. Phys. Solids **57**, 1880 (2009).
[4] M. D. Demetriou, M. Launey, G. Garrett, J. Schramm, D. Hofmann, W. Johnson, and R. O. Ritchie, Nat. Mater. **10**, 123 (2011).
[5] X. K. Xi, D. Q. Zhao, M. X. Pan, W. H. Wang, Y. Wu, and J. J. Lewandowski, Phys. Rev. Lett. **94**, 125510 (2005).
[6] G. Wang, Y. T. Wang, Y. H. Liu, M. X. Pan, D. Q. Zhao, and W. H. Wang, Appl. Phys. Lett. **89**, 121909 (2006).
[7] G. Wang, D. Q. Zhao, H. Y. Bai, M. X. Pan, A. L. Xia, B. S. Han, X. K. Xi, Y. Wu, and W. H. Wang, Phys. Rev. Lett. **98**, 235501 (2007).
[8] G. Wang, K. C. Chan, X. H. Xu, and W. H. Wang, Acta Mater. **56**, 5845 (2008).
[9] Y. T. Wang, G. Wang, X. X. Xia, and W. H. Wang, J. Appl. Phys. **106**, 113528 (2009).
[10] X. X. Xia and W. H. Wang, Small **8**, 1197 (2012).
[11] R. Narayan, P. Tandaiya, R. Narasimhan, and U. Ramamurty, Acta Mater. **80**, 407 (2014).
[12] R. Narasimhan, P. Tandaiya, I. Singh, R. Narayan, and U. Ramamurty, Int. J. Fract. **191**, 53 (2015).
[13] P. Murali, T. F. Guo, Y. W. Zhang, R. Narasimhan, Y. Li, and H. J. Gao, Phys. Rev. Lett. **107**, 215501 (2011).
[14] Y. Huang, J. W. Hutchinson, and V. Tvergaard, J. Mech. Phys. Solids **39**, 223 (1991).
[15] H. S. Hou and R. Abeyaratne, J. Mech. Phys. Solids **40**, 571 (1992).
[16] A. G. Varias, Z. Suo, and C. F. Shih, J. Mech. Phys. Solids **39**, 963 (1991).
[17] F. Celarie, S. Prades, D. Bonamy, L. Ferrero, E. Bouchaud, C. Guillot, and C. Marliere, Phys. Rev. Lett. **90**, 075504 (2003).
[18] J. P. Guin and S. M. Wiederhorn, Phys. Rev. Lett. **92**, 215502 (2004).
[19] Z. Lu, K. I. Nomura, A. Sharma, W. Wang, C. Zhang, A. Nakano, R. Kalia, P. Vashishta, E. Bouchaud, and C. Rountree, Phys. Rev. Lett. **95**, 135501 (2005).
[20] Y. C. Chen, Z. Lu, K. I. Nomura, W. Wang, R. K. Kalia, A. Nakano, and P. Vashishta, Phys. Rev. Lett. **99**, 155506 (2007).
[21] D. Bonamy, S. Prades, C. L. Rountree, L. Ponson, D. Dalmas, E. Bouchaud, K. Ravi-Chandar, and C. Guillot, Int. J. Fract. **140**, 3 (2006).
[22] C. Rountree, S. Prades, D. Bonamy, E. Bouchaud, R. Kalia, and C. Guillot, J. Alloys Compd. **434–435**, 60 (2007).
[23] C. Guerra, J. Scheibert, D. Bonamy, and D. Dalmas, Proc. Natl. Acad. Sci. U.S.A. **109**, 390 (2012).
[24] X. Zhou and C. Chen, Comput. Mater. Sci. **117**, 188 (2016).
[25] I. Singh, T. F. Guo, P. Murali, R. Narasimhan, Y. W. Zhang, and H. J. Gao, J. Mech. Phys. Solids **61**, 1047 (2013).
[26] I. Singh, T. Guo, R. Narasimhan, and Y. Zhang, Int. J. Solids Struct. **51**, 4373 (2014).
[27] C. H. Rycroft and E. Bouchbinder, Phys. Rev. Lett. **109**, 194301 (2012).
[28] D. L. Henann and L. Anand, Acta Mater. **57**, 6057 (2009).
[29] T. L. Andersson, *Fracture Mechanics: Fundamentals and Applications, Third Edition* (CRC Press, Taylor and Francis Group, Boca, Raton, FL, 2005).
[30] L. Anand and C. Su, J. Mech. Phys. Solids **53**, 1362 (2005).
[31] P. Tandaiya, U. Ramamurty, and R. Narasimhan, Model. Simul. Mater. Sci. Eng. **19**, 015002 (2011).
[32] C. Su and L. Anand, Acta Mater. **54**, 179 (2006).
[33] P. Tandaiya, R. Narasimhan, and U. Ramamurty, Acta Mater. **61**, 1558 (2013).
[34] C. A. Schuh and A. C. Lund, Nat. Mater. **2**, 449 (2003).
[35] A. Greer, Y. Cheng, and E. Ma, Mater. Sci. Eng. R **74**, 71 (2013).
[36] See Supplemental Material at http://link.aps.org/supplemental/10.1103/PhysRevLett.117.044302 for additional information about modeling aspects, the constitutive model and material parameters used in this Letter, along with a simulation movie, which includes Refs. [37].
[37] C. A. Schuh, T. C. Hufnagel, and U. Ramamurty, Acta Mater. **55**, 4067 (2007).
[38] A. A. Benzerga and J.-B. Leblond, in *Advances in Applied Mechanics*, Vol. 44 (Elsevier, New York, 2010), pp. 169–305.
[39] Y. Shao, G.-N. Yang, K.-F. Yao, and X. Liu, Appl. Phys. Lett. **105**, 181909 (2014).
[40] R. Maaß, P. Birckigt, C. Borchers, K. Samwer, and C. Volkert, Acta Mater. **98**, 94 (2015).
[41] V. Tvergaard and J. W. Hutchinson, Int. J. Solids Struct. **39**, 3581 (2002).
[42] J. Kim, X. Gao, and T. Srivatsan, Int. J. Solids Struct. **40**, 7357 (2003).
[43] J. W. Hutchinson, J. Mech. Phys. Solids **16**, 337 (1968).
[44] J. R. Rice and G. F. Rosengren, J. Mech. Phys. Solids **16**, 1 (1968).